





Tunneling electron induced luminescence from indium films on Si(111)Kenta Kuroishi , Hiroshi Okuyama *, Shinichiro Hatta , and Tetsuya Aruga *Department of Chemistry, Graduate School of Science, Kyoto University, Kyoto 606-8502, Japan*

(Received 18 March 2024; accepted 23 May 2024; published 10 June 2024)

We investigated the growth, electronic states, and tunneling electron induced luminescence of In ultrathin films on Si(111) using scanning tunneling microscopy (STM). The In films (4–8 monolayers) grew layer by layer by deposition at ~ 100 K. The dI/dV_s spectra exhibited the quantum-well states confined in the films. We observed luminescence originating from the junction plasmon excited via electron tunneling into the quantum-well state. Thus, by adjusting the thickness of the film at a single-layer level, we were able to modify the photon emission from the STM junction.

DOI: [10.1103/PhysRevB.109.235410](https://doi.org/10.1103/PhysRevB.109.235410)**I. INTRODUCTION**

Metallic thin films have attracted fundamental interest due to their unique electronic properties. Because of electron confinement in the direction normal to the surface, discrete electronic states called quantum-well states (QWSs) are formed, and their energies crucially depend on the film thickness [1]. As a result, the film thickness affects various surface properties such as the work function [2,3] and chemical reactivity [4,5] at a level of atomic layers.

The optical property of metallic thin films has been investigated by the luminescence spectroscopy from the junction of scanning tunneling microscopy (STM) [6–11]. The photon emission occurs via the inelastic electron tunneling (IET) mechanism, in which tunneling electrons excite the localized junction plasmon followed by radiative decay [12–16]. In this process, the electronic properties of metal thin film influence the luminescence spectra because the probability of the IET process depends on the density of states involved in the transition [17–30]. This implies that the QWSs play a crucial role in the luminescence properties of the films so that the spectra depend sensitively on the film thickness. The STM induced luminescence (STML) was reported for the single and double layers of Na films on Cu(111), where the QWSs were proposed to be involved in the transition [19]. However, there has been no study investigating the influence of QWS on STML across a broad range of film thicknesses.

The ($\sqrt{7} \times \sqrt{3}$) structure of In on Si(111) is known as a In double-layer film with free-electronlike metallic states [31]. The In atoms are arranged in a quasirectangular configuration which is reminiscent of the (001) planes of bulk In with a body-centered tetragonal (bct) lattice [32,33]. Further deposition of In at room temperatures induces the growth of three-dimensional crystals on the double layer [34], while a triple-layer structure is formed by the deposition below ~ 200 K [35–37]. The STM observation of the triple layer showed an (11×11) periodicity and quasi- (5.5×5.5) mod-

ulation, which is attributed to the moiré pattern between the lattices of Si(111) and In hexagonal packed layers [37]. The previous study for the thicker films also reported that the deposited films have the face-centered cubic (fcc) structure and (111) orientation [38].

In this paper, we report the growth, electronic states, and STML of the In ultrathin films by using STM. The In films grow in a layer-by-layer fashion at ~ 100 K up to eight layers, which showed distinct QWSs as a function of the thickness. We observed photon emission due to IET to the QWSs, thus manipulating the STML property of the films at a single-layer level.

II. EXPERIMENTAL METHODS

All the experiments were conducted at 78 K in an ultrahigh vacuum chamber (USM1200, Unisoku) with base pressure $< 1.5 \times 10^{-10}$ Torr. An electrochemically etched Ag tip and a mechanically polished PtIr tip were used for STM experiments, and the former was used for recording STML spectra. The topographic images were acquired in the constant-current mode with the sample bias voltage V_s and tunneling current I . The scanning tunneling (dI/dV_s) spectra were obtained by the lock-in technique with a modulation voltage of 20 mV_{rms} at 560.5 Hz. The STML spectra were recorded with constant current $I = 5$ nA for 60 s as a function of V_s . Emitted light was collected by a plano-convex lens mounted on the STM head and detected outside the chamber [39] by a charge-coupled device camera (Andor iDus420A) attached to a spectrograph (Andor KY193i). The tip apex was modified by voltage pulses and repeatedly contacted to the substrate to optimize its plasmonic response. The STML spectra were smoothed and subtracted by the background spectrum taken with the tip retracted.

Si(111) substrates were cut from an *n*-type Si(111) wafer ($\rho < 0.02 \Omega \text{ cm}$) and cleaned by repeated flash annealing. In was deposited on the Si(111)- (7×7) surface from an evaporator made with an alumina crucible heated by a tungsten wire loop. First, the double-layer film [In/Si(111)- $\sqrt{7} \times \sqrt{3}$ -rect structure] was prepared by depositing an excess amount of

*Contact author: hokuyama@kuchem.kyoto-u.ac.jp

In at 300 K and postannealing at 650 K [31,40]. The triple layer of the (11×11) superstructure, hereafter referred to as the 3 ML film, was produced by additional deposition of In < 120 K [37]. Thicker films were produced by further deposition on the 3 ML film under similar temperature conditions to suppress the formation of three-dimensional In crystals rather than two-dimensional films. Although the sample had to be removed from a cold stage at 78 K for the deposition, we achieved the formation of multilayer films by minimizing the total time the sample left the stage. The temperature during the deposition was estimated to be ~ 100 K from the low-energy electron diffraction (LEED) experiment.

III. RESULT

Figure 1(a) shows that the In atomic film was grown on the 3 ML film. For the 3 ML film [3 in Fig. 1(a)], the corrugation of the (5.5×5.5) moiré pattern is seen [37]. The upper right region of the STM image is covered with a smooth film [4 in Fig. 1(a)]. The apparent height from the 3 ML film surface is 2.5 \AA , which is evidently smaller than the Si(111) step height (3.13 \AA). We therefore refer to the smooth film as the 4 ML film. The low-bias STM image of the 4 ML film [Fig. 1(b)] showed an array of protrusions with the periodicity of $(\sqrt{3} \times \sqrt{3})R30^\circ$ with respect to the Si(111) substrate. Further growth of the In films in a layer-by-layer fashion was observed up to 8 ML [Figs. 1(c)–1(e)] with the $(\sqrt{3} \times \sqrt{3})$ superstructure retained. It was confirmed by LEED that the $(\sqrt{3} \times \sqrt{3})$ multilayer structure was stable at < 120 K. On the other hand, the $(\sqrt{3} \times \sqrt{3})$ LEED pattern disappeared > 140 K, and then the $(\sqrt{7} \times \sqrt{3})$ LEED pattern of the double-layer film was restored at ~ 170 K, probably accompanied with the growth of three-dimensional In crystals.

We suggest that the multilayer films consist of the hexagonal monoatomic layers of In as depicted in Fig. 1(f). In this model, the atomic density of each layer is only $\sim 0.5\%$ higher than that of the (101) surface of bulk bct In. Considering the atomic distances of neighboring atoms in bct (3.25 and 3.38 \AA), we estimate the distance between the close-packed layers to be 2.7 \AA . This distance is roughly consistent with the observed height of the layers. A similar multilayer structure has been reported for the (In, Mg)/Si(111) $(\sqrt{3} \times \sqrt{3})$ structure consisting of two (In, Mg)-alloy and one In layers [41]. It is noted that our close-packed model also resembles the fcc (111) model proposed for the In thin film prepared on Si(111)- (7×7) [42]. However, the $(\sqrt{3} \times \sqrt{3})$ periodicity for the multilayer In films has never been reported.

Figure 2(a) shows dI/dV_s spectra recorded for films with thickness from 4 to 8 ML. The 4 ML film exhibited a sharp peak at 1.1 V with a satellite at $\sim 1.5 \text{ V}$. For the 5 and 6 ML films, two close peaks were observed at 0.4 and -0.4 V , respectively. In addition, similar double peaks and peaks with satellite features were observed for thicker films and at higher V_s , although there were some exceptions that could not be resolved. The peak energies (marks) were determined by fitting with Gaussian functions [39] and were displayed as a function of thickness in Fig. 2(b). It is easy to see that the observed states are divided into three sequences, each of which has lower energy as the layer number increases. The thickness-dependent behavior of states strongly suggests the

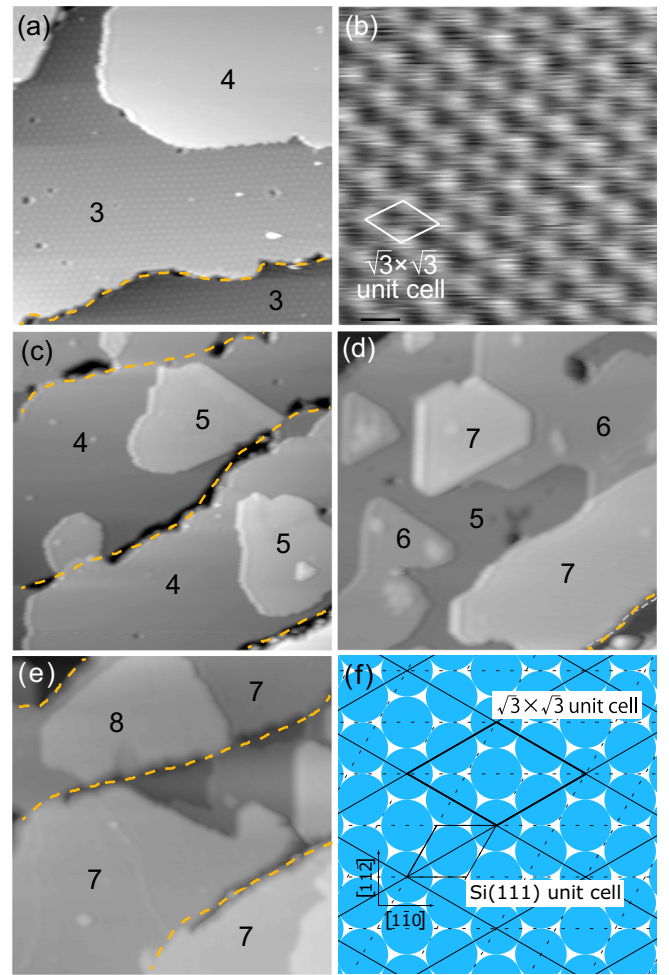


FIG. 1. (a) A scanning tunneling microscopy (STM) image of 3 and 4 ML In films on Si(111). The orange dashed line indicates the substrate step descending to the bottom right. (b) Enclosed image of the 4 ML film exhibiting $\sqrt{3} \times \sqrt{3}$ superstructure. (c)–(e) STM images of 4–8 ML In films on Si(111). The orange dashed lines indicate the substrate steps ascending to the bottom right. The images were acquired at (a) $I = 0.5 \text{ nA}$, $V_s = -0.8 \text{ V}$, (b) $I = 0.5 \text{ nA}$, $V_s = -0.3 \text{ V}$, (c) $I = 0.1 \text{ nA}$, $V_s = -1.0 \text{ V}$, (d) $I = 50 \text{ pA}$, $V_s = 0.5 \text{ V}$, and (e) $I = 40 \text{ pA}$, $V_s = 2.0 \text{ V}$. The image sizes are (a) $80 \times 80 \text{ nm}$, (b) $5.0 \times 5.0 \text{ nm}$, (c) $80 \times 80 \text{ nm}$, (d) $63 \times 63 \text{ nm}$, and (e) $90 \times 90 \text{ nm}$. (f) A model of the In films. The blue circles represent In atoms in the top layer. The dotted and solid lines represent (1×1) and $(\sqrt{3} \times \sqrt{3})$ lattices with respect to Si(111), respectively.

QWSs of electrons confined along the normal direction of the film [Fig. 2(c)]. On the other hand, the doublet features are attributed to the in-plane band structure of the QWSs [43]. The QWS around the $\bar{\Gamma}$ point is mainly composed of the In $5p_z$ orbital and exhibits upward dispersion. As the wave vector approaches the zone boundary, the hybridization of the $5p_z$ and $5p_{xy}$ orbitals alter the dispersion downward. The change in dispersion leads to two maxima in the density of states of the QWS. Therefore, the lower and higher energy peaks in close proximity correspond to the QWSs at the $\bar{\Gamma}$ and near the zone boundary, respectively. Similar double-peak features in STS were reported for the QWS of Pb thin films [44].

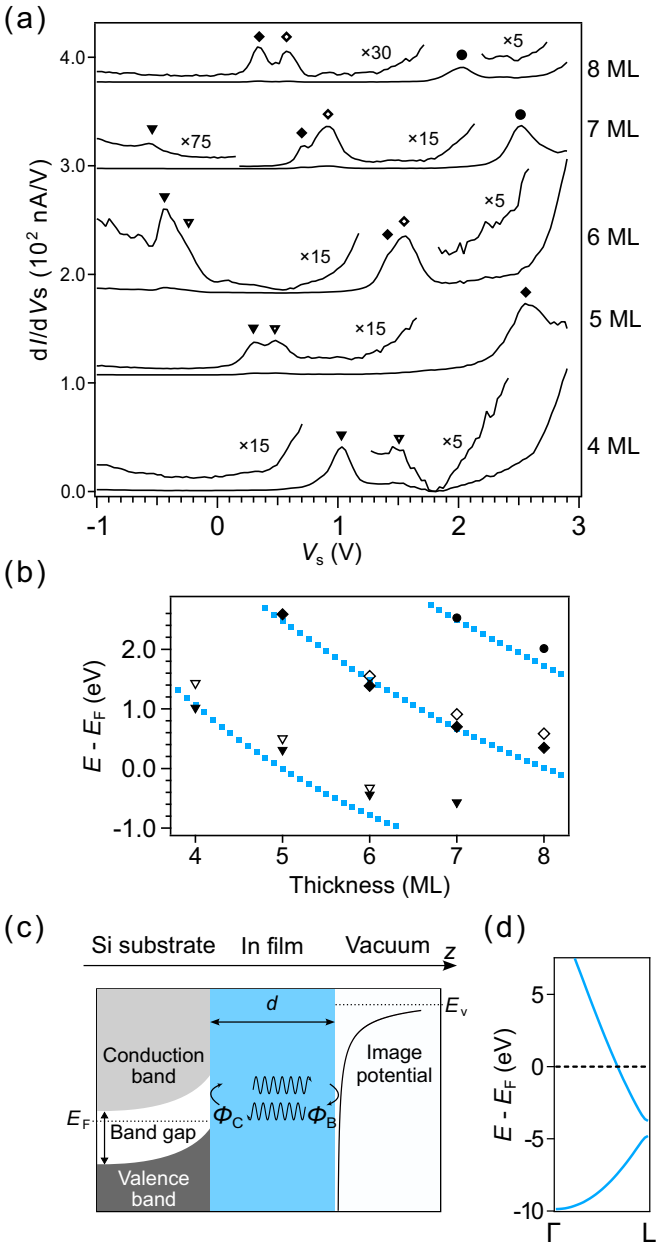


FIG. 2. (a) dI/dV_s spectra recorded for the In films as a function of the thickness (raw data). The spectra, except for the 4 ML, are offset vertically. The marks indicate peak positions determined by the decomposition. The tip height was fixed at the set point of $I = 0.5$ nA and $V_s = 1.0$ V. (b) The energies of the quantum-well state (QWS) as a function of the thickness. The marks and blue dotted curves indicate the experimental data and the calculated results, respectively. (c) A schematic illustration of the QWS in the In films on Si(111). (d) The calculated band structure of bulk In along the Γ -L direction.

The QWS are argued by using the phase accumulation (PA) model [45–47]. In the PA model, confined electrons produce standing-wave eigenstates in the condition:

$$2k_{\perp}d + \Phi_C + \Phi_B = 2m\pi, \quad (1)$$

where k_{\perp} and d represent the wave number in the direction perpendicular to the surface and the film thickness,

respectively [47,48]. Here, Φ_C and Φ_B are the phase shifts at the In/Si(111) and In/vacuum interfaces, respectively.

We simulated the energies of the QWSs as a function of the film thickness by using the PA model as follows. We assumed that the films consist of fcc-stacked In layers and electrons are confined in the Γ -L direction. The Γ -L dispersion was calculated with the generalized gradient approximation [49] to density functional theory, and we used the projector-augmented wave method implemented in QUANTUM ESPRESSO [50]. A plane-wave cutoff of 60 Ry was used. The fcc structure of In was relaxed with the lattice constant before the band calculation. As a result, we obtained a nearly free-electronlike band shown in Fig. 2(d) and the Fermi wave number of 1.54 \AA^{-1} . We used the wave number k_{\perp} with respect to that at L point [51,52] and assumed the linear dispersion relation at the Fermi level (E_F) [53]. The film thickness d is expressed as $d = Na + d_0$, where N is number of layers (ML), a is the interlayer distance of 2.7 \AA , and d_0 is an offset spacing used as a fitting parameter. The substrate-side phase shift Φ_C was tentatively fixed at π . The vacuum-side phase shift Φ_B is associated with the image potential barrier and is described as $\Phi_B = \pi\sqrt{3.4}/(E_v - E) - \pi$ [47,54,55], where E_v denotes the vacuum level ($E_v = E_F + 4.5 \text{ eV}$ [56,57]), and the energies are represented in units of eV.

Accordingly, we obtained the energies of the QWS from Eq. (1) and fitted them to the experimental results by using d_0 as a parameter [Fig. 2(b)]. The results are shown by blue dotted curves ($d_0 = -0.67 \text{ \AA}$). The marks correspond to the dI/dV_s peaks in Fig. 2(a). As a result, the PA model reproduced the dI/dV_s peak positions well at the energy > 1 eV. The deviation around E_F may be ascribed to the neglect of energy dependence of Φ_C .

Figure 3(a) shows STML spectra measured on the 7 ML film as a function of V_s from +2.0 to +5.0 V. The spectra between 2.8 and 4.2 V show a peak which shifts to higher energy with V_s . A second peak appears in the spectra for $V_s \geq 4.6$ V. The STML spectra were obtained as a function of the film thickness and presented as intensity maps in Fig. 3(b). The white solid lines represent the quantum cutoff ($\hbar\omega = |eV_s|$) which corresponds to a maximum photon energy supplied by a tunneling electron [13]. We did not observe photon emission via the two-electron process in which photon energy exceeds the quantum cutoff because this process requires tunnel current $> 1 \mu\text{A}$ [58–60]. Each map has an emission band whose photon energy increases linearly with V_s . The second peaks appear as relatively weak bands at $V_s = 4$ –5 V in the maps for 7 and 8 ML.

The STML can originate from the IET process with the excitation of the localized junction plasmon and the subsequent radiative decay of the plasmon. For the In films, the IET process predominantly occurs to the QWSs due to the large density of states. Therefore, the photon energy is given by a difference between E_F of the tip and the energy of the QWS as

$$\hbar\omega = eV_s - E_{\text{QWS}}, \quad (2)$$

where E_{QWS} represents the QWS energy with respect to E_F . Here, $\hbar\omega$ and e are the photon energy and the elementary charge, respectively. With the E_{QWS} determined in Fig. 2(a), we plot Eq. (2) with blue dotted lines in Fig. 3(b). The marks

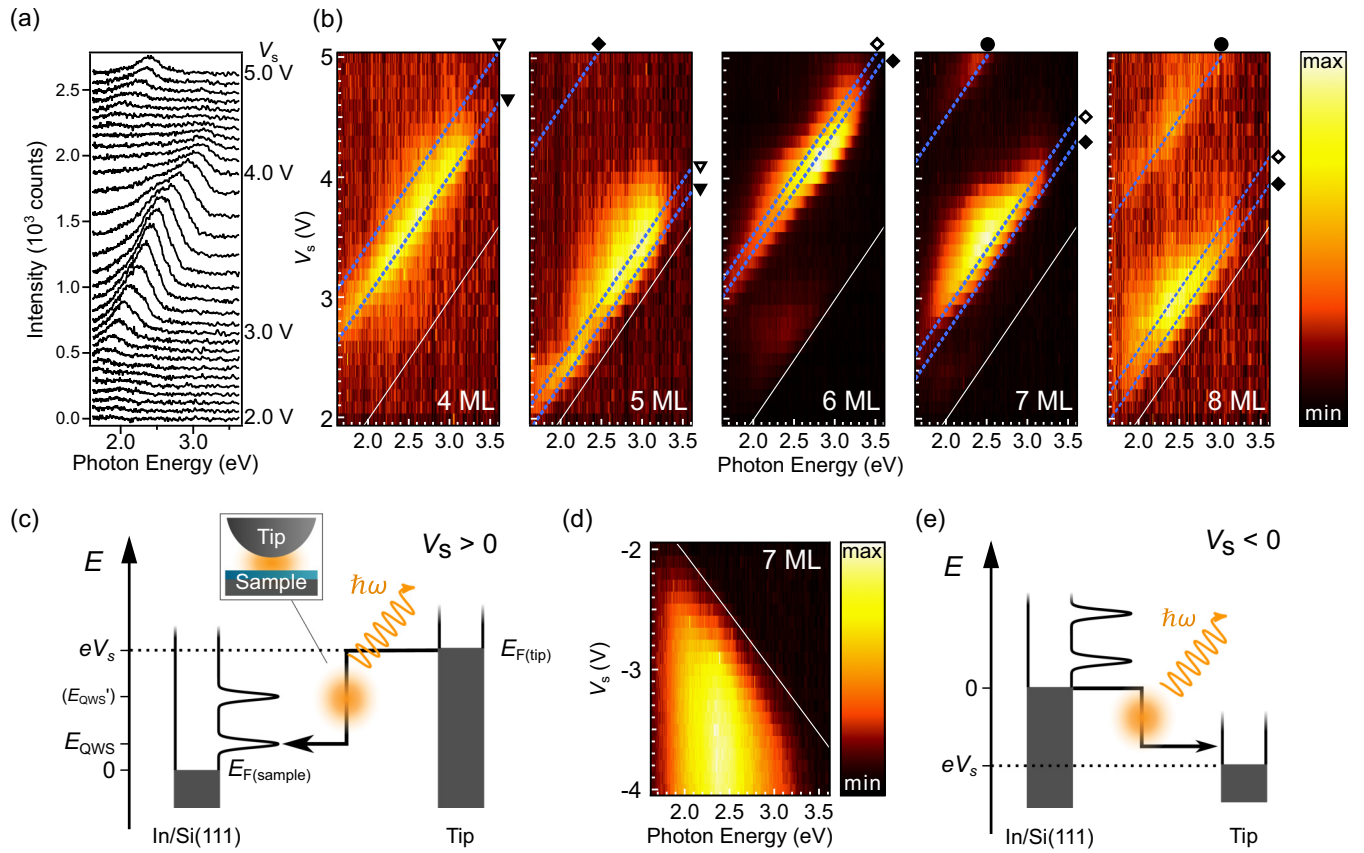


FIG. 3. (a) Scanning tunneling microscopy induced luminescence (STML) spectra of the 7 ML film as a function of V_s from 2.0 to 5.0 V at an interval of 0.1 V. They were recorded at $I = 5$ nA for 60 s. The spectra except the bottom one are offset vertically. (b) STML intensity maps for the film thickness from 4 to 8 ML as a function of V_s (2.0–5.0 V at a 0.1 V interval) and photon energy ($I = 5$ nA for 60 s). The maximum values of the scale are 550 counts for 4 ML, 650 counts for 5 ML, 3100 counts for 6 ML, 2000 counts for 7 ML, and 450 counts for 8 ML. The intensity depends on the condition of the tip apex. The white solid lines represent the relation of the quantum cutoff ($\hbar\omega = |eV_s|$). The blue dotted lines indicate the relation between V_s and photon energy given by the Eq. (2). (c) A schematic illustration of the inelastic electron tunneling (IET) process to quantum-well state (QWS) and excitation of the junction plasmon at positive V_s . (d) An STML intensity map of the 7 ML film recorded at negative V_s with the same condition as (b). The maximum value of the scale is 1600 counts. The white line indicates the relation of the quantum cutoff. (e) A schematic illustration of the excitation of the junction plasmon at negative V_s .

correspond to those in Fig. 2(a). Thus, the IET mechanism reproduces the observed photon energies. The intensities of the emission bands are strong ~ 2 – 3 eV and decrease away from this range. This is consistent with the junction mode of Ag tips [25]. It is noted that the doublet feature in the density of states does not necessarily cause the photon emission of equal intensity. For example, for the 5 ML film, the doublet [∇ and \blacktriangledown in Fig. 2(a)] results in the predominant photon emission for the former [Fig. 3(b)]. This implies that the probability of plasmon excitation via the IET process is not simply correlated with the local density of states but depends on the in-plane wave number of the QWS to which electrons tunnel. The underlying mechanism requires further elucidation through theoretical investigation. At negative V_s [Fig. 3(d)], the emission appears according to the quantum cutoff condition ($\hbar\omega \leq |eV_s|$), and no emission caused by the QWS was observed. This is illustrated in Fig. 3(e), and the absence of the QWS-related emission is consistent with that the QWS exists predominantly above E_F . The emission due to quantum cutoff appears weakly for positive V_s at 6 and 7 ML [Fig. 3(b)].

The STML induced by the interband transition between the QWSs was previously observed for Na layers on Cu(111) [19]. The interband emission is characterized by the constant photon energy as a function of V_s , which was not observed for the In films on Si(111) [Fig. 3(b)]. We suggest that the emission through the interband transition competes with the decay of tunneling electrons into the conduction band of Si(111), leading to its suppression. The projected band gap of Si(111) (2.4 eV at $\bar{\Gamma}$ [61]) is smaller than that of Cu(111) (>4 eV [62]), and thus, the QWS energy is out of the band gap for Si(111). Therefore, the energy position of the QWS with respect to the substrate electronic states may be crucial for the photon emission via interband transitions.

IV. SUMMARY

We have studied the growth, electronic properties, and STML of the In ultrathin films on Si(111) using STM. The films showed layer-by-layer growth and are suggested to consist of hexagonal packed layers. We observed the QWS and

related photon emission from the In layers as a function of thickness up to 8 ML. Consequently, the STML property of the ultrathin films was controlled by the number of the atomic layers.

ACKNOWLEDGMENTS

This paper was supported by JSPS KAKENHI Grants No. 21H01886, No. 21K18202, and No. 22K05036 and JST CREST Grant No. JPMJCR20R4.

- [1] R. C. Jaklevic and J. Lambe, Experimental study of quantum size effects in thin metal films by electron tunneling, *Phys. Rev. B* **12**, 4146 (1975).
- [2] F. K. Schulte, A theory of thin metal films: Electron density, potentials and work function, *Surf. Sci.* **55**, 427 (1976).
- [3] J. J. Paggel, C. M. Wei, M. Y. Chou, D.-A. Luh, T. Miller, and T.-C. Chiang, Atomic-layer-resolved quantum oscillations in the work function: Theory and experiment for Ag/Fe(100), *Phys. Rev. B* **66**, 233403 (2002).
- [4] P. J. Rous, Controlling the lifetime of adsorbate negative ion states, *Phys. Rev. Lett.* **83**, 5086 (1999).
- [5] A. G. Danese, F. G. Curti, and R. A. Bartynski, Quantum size effect induced modification of the chemisorption properties of thin metal films, *Phys. Rev. B* **70**, 165420 (2004).
- [6] J. K. Gimzewski, J. K. Sass, R. R. Schlitter, and J. Schott, Enhanced photon emission in scanning tunnelling microscopy, *Europhys. Lett.* **8**, 435 (1989).
- [7] R. Nishitani, T. Umeno, and A. Kasuya, A study of metal films using a spectrally resolved photon map obtained by spectrum mapping measurements of STM-induced light, *Appl. Phys. A* **66**, S139 (1998).
- [8] Y. Suzuki, H. Minoda, and N. Yamamoto, STM light emission from Ag/Si(111), *Surf. Sci.* **438**, 297 (1999).
- [9] D. G. Walmsley, T.-S. Tan, and P. Dawson, Light emission from gold and silver thin films in a scanning tunneling microscope: Role of contamination and interpretation of grain structure in photon maps, *Surf. Sci.* **572**, 497 (2004).
- [10] H. Imada, A. Chiba, M. Yokoya, and N. Yamamoto, STM light emission from Si (111)-7 × 7 and Si (111)-4 × 1-In surfaces: Optical investigation with atomic resolution, *Microsc. Microanal.* **13**, 806 (2007).
- [11] V. A. Shkoldin, D. V. Permyakov, K. S. Ladutenko, M. V. Zhukov, A. A. Vasiliev, A. O. Golubok, A. V. Uskov, A. D. Bolshakov, A. A. Bogdanov, A. K. Samusev *et al.*, Crucial role of metal surface morphology in photon emission from a tunnel junction at ambient conditions, *J. Phys. Chem. C* **123**, 8813 (2019).
- [12] J. Lambe and S. L. McCarthy, Light emission from inelastic electron tunneling, *Phys. Rev. Lett.* **37**, 923 (1976).
- [13] R. Berndt, J. K. Gimzewski, and P. Johansson, Inelastic tunneling excitation of tip-induced plasmon modes on noble-metal surfaces, *Phys. Rev. Lett.* **67**, 3796 (1991).
- [14] K. Kuhnke, C. Große, P. Merino, and K. Kern, Atomic-scale imaging and spectroscopy of electroluminescence at molecular interfaces, *Chem. Rev.* **117**, 5174 (2017).
- [15] F. Rossel, M. Pivetta, and W.-D. Schneider, Luminescence experiments on supported molecules with the scanning tunneling microscope, *Surf. Sci. Rep.* **65**, 129 (2010).
- [16] R. J. Peña Román, Y. Auad, L. Grasso, L. A. Padilha, F. Alvarez, I. D. Barcelos, M. Kociak, and L. F. Zagonel, Design and implementation of a device based on an off-axis parabolic mirror to perform luminescence experiments in a scanning tunneling microscope, *Rev. Sci. Instrum.* **93**, 043704 (2022).
- [17] R. Berndt and J. K. Gimzewski, Isochromat spectroscopy of photons emitted from metal surfaces in an STM, *Ann. Phys. (Berlin)* **505**, 133 (1993).
- [18] S. Kagami, H. Minoda, and N. Yamamoto, STM light emission from Si(111) $\sqrt{3} \times \sqrt{3}$ -Ag surface, *Surf. Sci.* **493**, 78 (2001).
- [19] G. Hoffmann, J. Kliewer, and R. Berndt, Luminescence from metallic quantum wells in a scanning tunneling microscope, *Phys. Rev. Lett.* **87**, 176803 (2001).
- [20] G. Hoffmann, J. Kröger, and R. Berndt, Color imaging with a low temperature scanning tunneling microscope, *Rev. Sci. Instrum.* **73**, 305 (2002).
- [21] G. V. Nazin, X. H. Qiu, and W. Ho, Atomic engineering of photon emission with a scanning tunneling microscope, *Phys. Rev. Lett.* **90**, 216110 (2003).
- [22] G. Schull, M. Becker, and R. Berndt, Imaging confined electrons with plasmonic light, *Phys. Rev. Lett.* **101**, 136801 (2008).
- [23] T. Lutz, C. Große, C. Dette, A. Kabachiev, F. Schramm, M. Ruben, R. Gutzler, K. Kuhnke, U. Schlickum, and K. Kern, Molecular orbital gates for plasmon excitation, *Nano Lett.* **13**, 2846 (2013).
- [24] A. Stróżecka, J. Li, R. Schürmann, G. Schulze, M. Corso, F. Schulz, C. Lotze, S. Sadewasser, K. J. Franke, and J. I. Pascual, Electroluminescence of copper-nitride nanocrystals, *Phys. Rev. B* **90**, 195420 (2014).
- [25] J. Martínez-Blanco and S. Fölsch, Light emission from Ag(111) driven by inelastic tunneling in the field emission regime, *J. Phys.: Condens. Matter* **27**, 255008 (2015).
- [26] N. Krane, C. Lotze, J. M. Läger, G. Reecht, and K. J. Franke, Electronic structure and luminescence of quasi-freestanding MoS₂ nanopatches on Au(111), *Nano Lett.* **16**, 5163 (2016).
- [27] A. Yu, S. Li, G. Czap, and W. Ho, Tunneling-electron-induced light emission from single gold nanoclusters, *Nano Lett.* **16**, 5433 (2016).
- [28] M. C. Cottin, E. Ekici, and C. A. Bobisch, STM-induced light emission enhanced by weakly coupled organic ad-layers, *Appl. Phys. Lett.* **112**, 101602 (2018).
- [29] A. Yu, S. Li, H. Wang, S. Chen, R. Wu, and W. Ho, Visualization of nanoplasmonic coupling to molecular orbital in light emission induced by tunneling electrons, *Nano Lett.* **18**, 3076 (2018).
- [30] K. Edelmann, L. Wilmes, V. Rai, L. Gerhard, L. Yang, M. Wegener, T. Repán, C. Rockstuhl, and W. Wulfhekel, Influence of Co bilayers and trilayers on the plasmon-driven light emission from Cu(111) in a scanning tunneling microscope, *Phys. Rev. B* **101**, 205405 (2020).
- [31] E. Rotenberg, H. Koh, K. Rosnagel, H. W. Yeom, J. Schäfer, B. Krenzer, M. P. Rocha, and S. D. Kevan, Indium $\sqrt{7} \times \sqrt{3}$ on Si(111): A nearly free electron metal in two dimensions, *Phys. Rev. Lett.* **91**, 246404 (2003).

- [32] J. W. Park and M. H. Kang, Double-layer In structural model for the In/Si(111)- $\sqrt{7} \times \sqrt{3}$ surface, *Phys. Rev. Lett.* **109**, 166102 (2012).
- [33] T. Shirasawa, S. Yoshizawa, T. Takahashi, and T. Uchihashi, Structure determination of the Si(111)- $\sqrt{7} \times \sqrt{3}$ -In atomic-layer superconductor, *Phys. Rev. B* **99**, 100502(R) (2019).
- [34] S. L. Surnev, J. Kraft, and F. P. Netzer, Modification of overlayer growth kinetics by surface interlayers: The Si(111)- $\sqrt{7} \times \sqrt{3}$ -indium surface, *J. Vac. Sci. Technol. A* **13**, 1389 (1995).
- [35] M. Xu, X.-M. Dou, J.-F. Jia, Q.-K. Xue, Y. Zhang, A. Okada, S. Yoshida, and H. Shigekawa, Scanning tunneling microscopy observation of surface superstructures during the growth of In on In/Si(111) surface, *Thin Solid Films* **520**, 328 (2011).
- [36] T. Suzuki and K. Yagyu, Formation of the incommensurate Si(111)- $\sim 5.4 \times \sim 5.4$ -In surface, *Surf. Sci.* **726**, 122174 (2022).
- [37] S. Hatta, K. Kuroishi, K. Yukawa, T. Murata, H. Okuyama, and T. Aruga, Moiré superlattice and two-dimensional free-electron-like states of indium triple-layer structure on Si(111), *Phys. Rev. B* **108**, 045427 (2023).
- [38] J. H. Dil, B. Hülsen, T. U. Kampen, P. Kratzer, and K. Horn, Influence of the substrate lattice structure on the formation of quantum well states in thin In and Pb films on silicon, *J. Phys.: Condens. Matter* **22**, 135008 (2010).
- [39] See Supplemental Material at <http://link.aps.org/supplemental/10.1103/PhysRevB.109.235410> for the schematic of the STML experiment and the peak decomposition of the spectra in Fig. 2(a).
- [40] J. Kraft, M. G. Ramsey, and F. P. Netzer, Surface reconstructions of In on Si(111), *Phys. Rev. B* **55**, 5384 (1997).
- [41] S. Terakawa, S. Hatta, H. Okuyama, and T. Aruga, Ultrathin (In, Mg) films on Si(111): A nearly freestanding double-layer metal, *Phys. Rev. B* **105**, 125402 (2022).
- [42] Y. Liu, T. Miller, and T. C. Chiang, Electronic structure and trilayer growth of indium films on Si(111): A photoemission study, *J. Phys.: Condens. Matter* **23**, 365302 (2011).
- [43] J. H. Dil, T. U. Kampen, B. Hülsen, T. Seyller, and K. Horn, Quantum size effects in quasi-free-standing Pb layers, *Phys. Rev. B* **75**, 161401(R) (2007).
- [44] V. Cherkez, P. Mallet, T. Le Quang, L. Magaud, and J.-Y. Veuillen, Electronic properties of Pb islands on graphene: Consequences of a weak interface coupling from a combined STM and *ab initio* study, *Phys. Rev. B* **98**, 195441 (2018).
- [45] M. A. Mueller, A. Samsavar, T. Miller, and T.-C. Chiang, Probing interfacial properties with Bloch electrons: Ag on Cu(111), *Phys. Rev. B* **40**, 5845 (1989).
- [46] T.-C. Chiang, Photoemission studies of quantum well states in thin films, *Surf. Sci. Rep.* **39**, 181 (2000).
- [47] M. Milun, P. Pervan, and D. P. Woodruff, Quantum well structures in thin metal films: Simple model physics in reality? *Rep. Prog. Phys.* **65**, 99 (2002).
- [48] N. V. Smith, Phase analysis of image states and surface states associated with nearly-free-electron band gaps, *Phys. Rev. B* **32**, 3549 (1985).
- [49] J. P. Perdew, K. Burke, and M. Ernzerhof, Generalized gradient approximation made simple, *Phys. Rev. Lett.* **77**, 3865 (1996).
- [50] P. Giannozzi, S. Baroni, N. Bonini, M. Calandra, R. Car, C. Cavazzoni, D. Ceresoli, G. L. Chiarotti, M. Cococcioni, I. Dabo *et al.*, QUANTUM ESPRESSO: A modular and open-source software project for quantum simulations of materials, *J. Phys.: Condens. Matter* **21**, 395502 (2009).
- [51] J. E. Ortega, F. J. Himpsel, G. J. Mankey, and R. F. Willis, Quantum-well states and magnetic coupling between ferromagnets through a noble-metal layer, *Phys. Rev. B* **47**, 1540 (1993).
- [52] J. E. Ortega, F. J. Himpsel, G. J. Mankey, and R. F. Willis, Quantum well states in metallic thin layers, *Surf. Rev. Lett.* **04**, 361 (1997).
- [53] M. Becker and R. Berndt, Scattering and lifetime broadening of quantum well states in Pb films on Ag(111), *Phys. Rev. B* **81**, 205438 (2010).
- [54] E. G. McRae, Surface-state resonances in low-energy electron diffraction, *Surf. Sci.* **25**, 491 (1971).
- [55] E. G. McRae, Electronic surface resonances of crystals, *Rev. Mod. Phys.* **51**, 541 (1979).
- [56] F. G. Allen and G. W. Gobeli, Comparison of the photoelectric properties of cleaved, heated, and sputtered silicon surfaces, *J. Appl. Phys.* **35**, 597 (1964).
- [57] H. Hirayama, S. Baba, and A. Kinbara, Summary Abstract: The work function of In/Si(111) superstructures, *J. Vac. Sci. Technol. A* **4**, 1416 (1986).
- [58] N. L. Schneider, G. Schull, and R. Berndt, Optical probe of quantum shot-noise reduction at a single-atom contact, *Phys. Rev. Lett.* **105**, 026601 (2010).
- [59] F. Xu, C. Holmqvist, and W. Belzig, Overbias light emission due to higher-order quantum noise in a tunnel junction, *Phys. Rev. Lett.* **113**, 066801 (2014).
- [60] K. Kaasbjerg and A. Nitzan, Theory of light emission from quantum noise in plasmonic contacts: Above-threshold emission from higher-order electron-plasmon scattering, *Phys. Rev. Lett.* **114**, 126803 (2015).
- [61] D. Straub, L. Ley, and F. J. Himpsel, Conduction-band and surface-state critical points in Si: An inverse-photoemission study, *Phys. Rev. Lett.* **54**, 142 (1985).
- [62] J. A. Knapp, F. J. Himpsel, and D. E. Eastman, Experimental energy band dispersions and lifetimes for valence and conduction bands of copper using angle-resolved photoemission, *Phys. Rev. B* **19**, 4952 (1979).